Journal of Advances in Modeling Earth Systems

RESEARCH ARTICLE
10.1029/2017MS001239

The Impact of Vertical Mixing Biases in Large-Eddy Simulation on Nocturnal Low Clouds

B. J. H. van Stratum[1,2,3] and B. Stevens[1]

[1]Max Planck Institute for Meteorology, Hamburg, Germany, [2]International Max Planck Research School on Earth System Modelling, Hamburg, Germany, [3]Now at Royal Netherlands Meteorological Institute (KNMI), de Bilt, the Netherlands

Key Points:
- The impact of vertical mixing biases on nocturnal low clouds is studied using observations and newly developed conceptual model
- Overestimating vertical mixing is unlikely to produce low clouds in models, which do not occur in reality

Correspondence to:
B.J.H. van Stratum,
bart@vanstratum.com

Citation:
van Stratum, B. J. H., & Stevens, B. (2018). The impact of vertical mixing biases in large-eddy simulation on nocturnal low clouds. *Journal of Advances in Modeling Earth Systems*, *10*, 1290–1303. https://doi.org/10.1029/2017MS001239

Received 16 NOV 2017
Accepted 27 APR 2018
Accepted article online 5 MAY 2018
Published online 21 JUN 2018

Abstract The use of large-eddy simulation at a resolution insufficient to resolve the largest turbulent eddies frequently suffers from an overestimation of vertical mixing in the nocturnal boundary layer. The resulting biases in the mean thermodynamic structure—typically an overestimation of the near-surface temperature, and underestimation of the boundary layer top temperature—could potentially influence the formation of low clouds or fog. Whether this is likely to happen is assessed using both observations, and a newly developed conceptual model. First, observations from Northwestern Europe (Germany and Netherlands) are used to characterize the humidity conditions at night. The results indicate that saturation most likely occurs at the surface, but that the conditions at 200 m height are also often close to saturation. Second, the conceptual model is used to study whether overestimating vertical mixing, and the resulting negative temperature biases at the boundary layer top, could result in a spurious formation of low clouds in large-eddy simulations. The results convincingly indicate that this is unlikely to happen, as overestimating vertical mixing decreases the relative humidity throughout the nocturnal boundary layer.

1. Introduction

Large-eddy simulation (LES) is slowly moving from purposefully process studies to conditions that endeavor to be as realistic as possible. Examples include running LES continuously (days to years) forced by a weather model—and hence closely tied to the observed state—either to validate or develop convection parameterizations (Neggers et al., 2012), study long-term turbulence statistics (Schalkwijk et al., 2015a), or validate or compare LES with observations (Heinze et al., 2017). In addition, LES has recently been used to perform weather hindcasts on domains as large as the Netherlands ($\sim$400 $\times$ 400 km^2, Schalkwijk et al., 2015b) and Germany ($\sim$750 $\times$ 750 km^2, Heinze et al., 2016).

With traditional idealized LES experiments, the domain size ($\mathcal{L}$) and grid spacing (Δ) are typically adjusted for the process being studied, to keep the computational costs manageable. This results in a wide variety of LES setups, ranging from experiments with $\Delta\,\mathcal{O}(1\text{ m})$ and $\mathcal{L}\mathcal{O}$ (100 m) for studies of the nocturnal boundary layer (NBL, e.g., Beare et al., 2006), up to $\Delta\mathcal{O}$ (100 m) and $\mathcal{L}\mathcal{O}$ (100–1,000 km) for studies of deep convection (e.g., Hohenegger et al., 2015). The previously mentioned realistic experiments, when covering the full diel cycle, should (at least in theory) use a grid spacing of $\mathcal{O}(1\text{ m})$ to resolve the small nocturnal eddies, within a domain of $\mathcal{O}(100\text{ km})$ to allow for the development of the largest convective structures. As such experiments are computationally not feasible—both now and in the foreseeable future—often sacrifices are made, using a resolution which is sufficient to resolve daytime convection, but insufficient to resolve all turbulence at night (e.g., Schalkwijk et al., 2015a; van Stratum & Stevens, 2015).

In such a low-resolution LES setup (low-resolution with respect to the resolution required to resolve turbulence at night), the mean thermodynamic structure of the NBL is often poorly represented. There is some justification for this approach, as previous work has shown that for unsaturated conditions, the misrepresentation of the nighttime conditions has little impact on the following day of convection (van Stratum & Stevens, 2015, hereinafter: vSS15). However, the work of vSS15 only focused on the fundamental principle behind LES—turbulent mixing—and part of the robustness of the daytime evolution was shown to result from the fact that biases in vertical mixing did not substantially alter the nighttime energy balance. However, in the presence of moisture, biases in vertical mixing can influence, or offset other important processes, like the formation of fog or clouds (e.g., Duynkerke, 1999) or radiation (e.g., Edwards, 2009; Garratt &

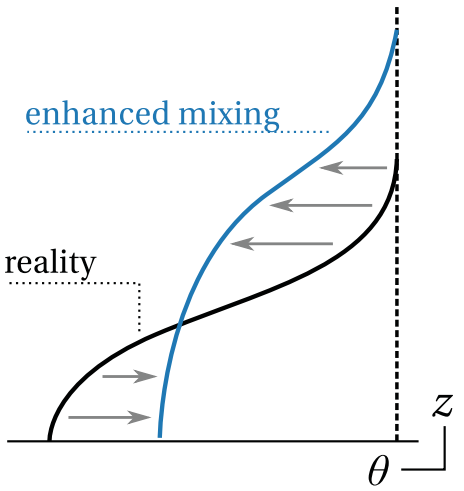

Figure 1. Typical NBL bias in low-resolution LES.

Brost, 1981). Especially the interaction between these two processes—the influence of clouds on radiation and the nighttime energy balance—has the potential to further modify the NBL development. In addition, if spurious nocturnal clouds persist into the early morning, a reduction in the incoming shortwave solar radiation can reduce the surface heating which drives the development of the convective boundary layer, potentially further influencing the onset or intensity of convection (Anber et al., 2015; Yin et al., 2015).

In low-resolution LES, as well as models based on the Reynolds Averaged Navier-Stokes (RANS) equations, vertical mixing is often overestimated at night (Cuxart et al., 2006; de Roode et al., 2017; Holtslag et al., 2013; Mauritsen et al., 2007), typically causing a positive temperature bias near the surface, and a negative temperature bias near/above the boundary layer top, as illustrated in Figure 1. This has the potential to influence fog or low clouds in two ways: (1) the positive temperature bias near the surface causes an absence of fog occurring in reality, and/or (2) the negative temperature bias aloft causes a spurious formation of low clouds.

We study how likely these biases in the formation of fog or low clouds occur, using both observations over Germany and the Netherlands, and a newly developed conceptual model. Like in vSS15, the main concern is whether nocturnal biases have the potential to influence the following day of convection. Therefore, the analysis is limited to the May through August period, and nights in between convective days. Although this leaves out the months in which fog most frequently occurs over Europe, this allows us to focus on the periods in which the use of LES is arguably most beneficial through its explicit representation of daytime convection. In addition, we focus on processes in the NBL, and neglect e.g., radiative processes at the top of the (residual) convective layer. The latter can be important for stratus or stratocumulus formation (Fitzjarrald & Lala, 1989), but we expect these conditions—by virtue of the scale of the eddies that are driven by this cooling—to be better handled by the LES model.

First, the observation from Cabauw in the Netherlands and two sites, Hamburg and Karlsruhe, in Germany are used to characterize the humidity conditions at night. Using the observations, several questions can be answered, for example how often the NBL saturates, where it saturates (near the surface or higher up), or how close the NBL gets to saturation. The latter can be especially important given the negative temperature biases near or above the NBL top (Figure 1).

Second, we address the question whether overestimating vertical mixing can cause a spurious formation of low clouds which do not occur in reality or the absence of mixing biases. When introducing moisture, the parameter space of an LES setup increases greatly compared to a setup without moisture, which complicates the design of a representative experiment, or set of experiments. For this reason we developed a conceptual model which—given the total nocturnal cooling (time integral of the surface heat flux over the nocturnal period) and the depth over which the cooled air is mixed—reproduces the vertical structure of the NBL for a variety of conditions. This work builds on a long tradition of using bulk (or idealized) concepts to model the atmospheric boundary layer, for convective (e.g., Betts, 1973; Lilly, 1968; Stevens, 2006; Tennekes, 1973) and stable (Stull, 1983a, 1983b; Van de Wiel et al., 2002) conditions, and study the moisture characteristics and evolution of such boundary layers (e.g., Ek & Mahrt, 1994; Fitzjarrald & Lala, 1989). We build on the work of Stull (1983a, 1983b), but derive a modified vertical NBL structure from LES experiments, which is more representative for the cases that are being considered, and the typical NBL structure produced by LES. Using the conceptual model we can study how overestimating vertical mixing influences the relative humidity for a wide range of conditions, using only a fraction of the computational resources that would be required to perform the same experiments with LES. In addition, the conceptual nature of the model allows us to develop a more fundamental understanding of how mixing biases influence the relative humidity in the NBL.

We start the observational study in section 2 with a description of the measurement sites, followed by the methods used for the selection and analysis of the relevant nights in section 2.2. In sections 2.3 and 2.4 the

general characteristics and extremes of the nocturnal conditions are discussed. The second part of this paper starts in section 3.1 with the derivation and validation of the conceptual model, followed by the numerical experiments in section 3.2. Finally, the paper is concluded in section 4.

2. Moisture Characteristics of European Summertime Nights

To quantify the humidity conditions of summertime nights, and the spatial differences across northwest Europe, we analyze data from three measurement sites (Figure 2). The sites at Cabauw, Hamburg, and Karlsruhe were selected because of the availability of tower measurements and the relative long observational records that are available for these sites: for this study 2001–2014 for Cabauw and Karlsruhe, and 2004–2012 for Hamburg. Although all three locations are in the same Köppen-Geiger climate classification, the characteristics of the sites are quite diverse.

2.1. Description Observation Sites

Hamburg is located in the northern part of Germany, 75–100 km from both the Baltic and North Sea. The weather mast (280 m high), operated by the University of Hamburg, is in close proximity to the city (53.52°N, 10.10°E), with adjacent industrial areas and community gardens, and more rural terrain toward the east (Brümmer et al., 2012). As shown in Figure 2, the prevailing winds in Hamburg are westerly, placing the observation site downwind of the city.

The Cabauw Experimental Site for Atmospheric Research (CESAR) is located in the western part of the Netherlands (51.97°N 4.93°E), at 40 km distance from the North Sea. The measurement site is located in a low (0.7 m above sea level) and flat polder, with the tower (200 m high) surrounded by relatively homogeneous open pasture and small drainage ditches (Van Ulden & Wieringa, 1996).

Karlsruhe is on the southwestern border between Germany and France. The measurement site (49.10°N, 8.43°E), operated by the Institute for Meteorology and Climate research—Karlsruhe Institute of Technology (KIT), is located in the relatively flat Rhine valley, but with stronger orography (Odenwald, Pfälzerwald, and Schwarzwald) in the near vicinity. As shown in Figure 2, this has a strong impact on the wind direction

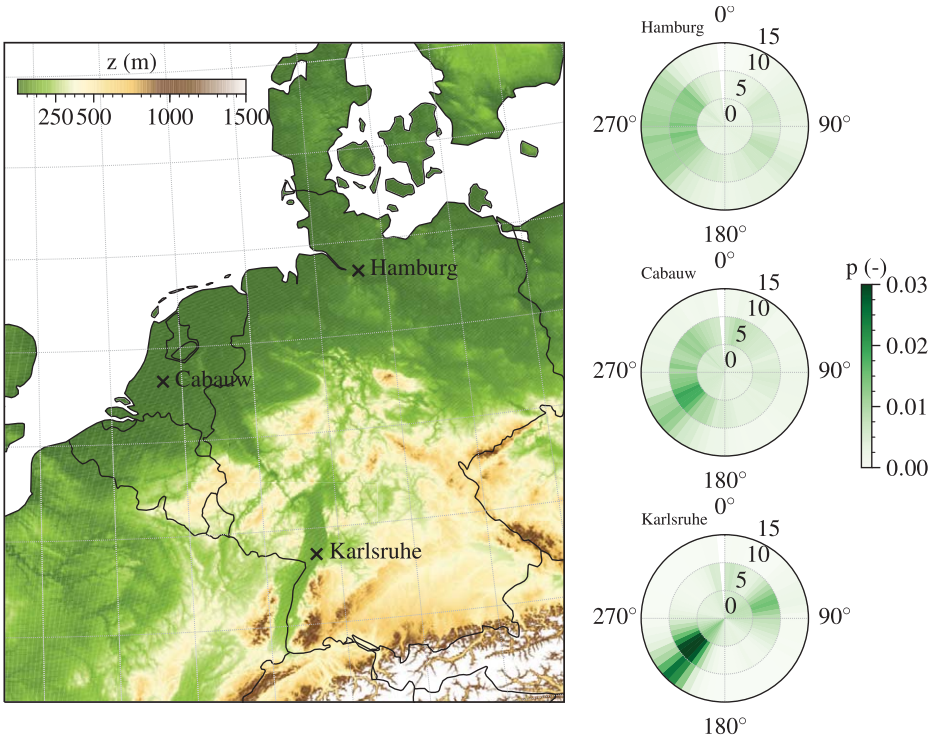

Figure 2. Map showing the location of the measurement sites and orography, with indication of the May through August wind direction of each measurement site.

Table 1
Statistics of the Measurement Sites

	T (K)	q (g kg^{-1})	N_{tot}	N_{samp}	f
Cabauw	290.1	8.3	1,722	867	0.50
Hamburg	291.6	7.5	1,099	530	0.48
Karlsruhe	296.3	8.4	1,709	958	0.56

Note. Median temperature (T) and specific humidity (q) at $\hat{t} = 0$, $z = 2$ m. N = total and sampled number of nights which are considered in the statistics, f the fraction N_{samp}/N_{tot}.

(Kalthoff & Vogel, 1992). The measurement tower (200 m high) is located in a pine forest, with the observations below 20 m collected at a small meadow directly north of the tower.

Given the location of the sites, certain relevant characteristics, like the soil moisture content, are expected to differ. As not all sites provide such observations, this could unfortunately not be included in the analysis. Furthermore, the two lowest observation levels for all sites are at 2 and 10 m height, because of which fine details in the NBL development might be missed in the analysis. High-resolution soundings could have improved this, but are not routinely available at the three selected sites.

2.2. Data Selection and Analysis Method

Because of the current study's interest in daytime convection, the analysis focuses on the summer (May through August) period. Compared to vSS15, who only analyzed data from clear (cloudless) nights, the sampling criteria is relaxed to nights in between relatively clear (and with that, most likely convective) days. This way, nights at which fog or low clouds occur are included in the analysis. The total and sampled number of nights are shown in Table 1, the sampling criteria and procedure is described in Appendix A. Unless stated otherwise, from this point on *nights* will refer to the sampled set of nighttime conditions.

For all nights, the temporal evolution of the NBL is studied over the period at which the lower atmosphere is stably stratified ($\theta_\rho^{10m} - \theta_\rho^{2m} > 0$, with θ_ρ the potential density temperature $\theta_\rho = \theta(1+0.61\ q)$). The first time in the evening at which this criteria is met is referred to as t_{N0}, the last time in the morning as t_{N1}, and the time in between is normalized as $\hat{t} = (t - t_{N0})/(t_{N1} - t_{N0})$. This ensures that the initial vertical profiles like the potential temperature and specific humidity are close to the (well-mixed) convective conditions, and the temporal evolution over the period $\hat{t} = \{0-1\}$ describes the deviation from the convective conditions. At or just after t_{N0}, the specific humidity often changes on very short timescales (Acevedo & Fitzjarrald, 2001; Fitzjarrald & Lala, 1989). Depending on the exact choice of t_{N0}, such abrupt changes might be excluded from the nighttime evolution. A sensitivity analysis on the exact choice of t_{N0} revealed that the results presented in this section are insensitive to small errors in the choice of t_{N0}. For Cabauw and Hamburg t_{N0} is on average 2.1 h before sunset, for Karlsruhe 2.8 h before sunset. The average night length ($t_{N1} - t_{N0}$) is 11.7 h for Hamburg, 12.4 h for Cabauw, and 13.3 h for Karlsruhe.

The analysis focuses on moisture related variables like the relative humidity (RH), dew point depression ($T - T_d$), and specific humidity (q). The selected variables are predominantly studied using two-dimensional histograms, with the normalized time $\hat{t}$ on the x-axis, and the probability on the y-axis, with the frequency within each time bin normalized to unity.

2.3. General Characteristics

The analysis starts with a comparison of the initial conditions, to differentiate initial differences from differences introduced during the nocturnal period. Next, the temporal evolution of the relative and specific humidity is described, and further studied using the relative humidity budget equation. Finally, extremes during the nocturnal period are discussed.

2.3.1. Onset of the NBL

As shown in Figures 3a–3c, the initial ($\hat{t} = 0$) relative humidity at 2 m decreases going further inland, from ~65% in Cabauw to ~52% in Hamburg and ~47% in Karlsruhe, thus showing differences of nearly 20% over a distance of 400 km. The variation between Cabauw and Kalrsruhe is mostly caused by a difference in temperature: the initial specific humidity is approximately the same for both sites, but the temperature differs > 6 K, as shown in Table 1. Although geographically Hamburg is at a higher latitude than Cabauw, the temperature at the beginning of the night is higher. This difference in temperature, and the lower specific humidity, might be explained by the close proximity of the measurement site to the city of Hamburg, and the local influence of cities on temperature (urban heat island, UHI, e.g., Barlow, 2014) and moisture (e.g., Kuttler et al., 2007). The variation in the initial conditions is similar for all three sites, with standard deviations in between 4.6 and 4.9 K for the potential temperature, and 2.1–2.6 g kg^{-1} for the specific humidity. At 200 m (Hamburg: 175 m) height, the initial conditions and differences between the sites are very similar, since at $\hat{t} = 0$ the boundary layer is still close to being well mixed.

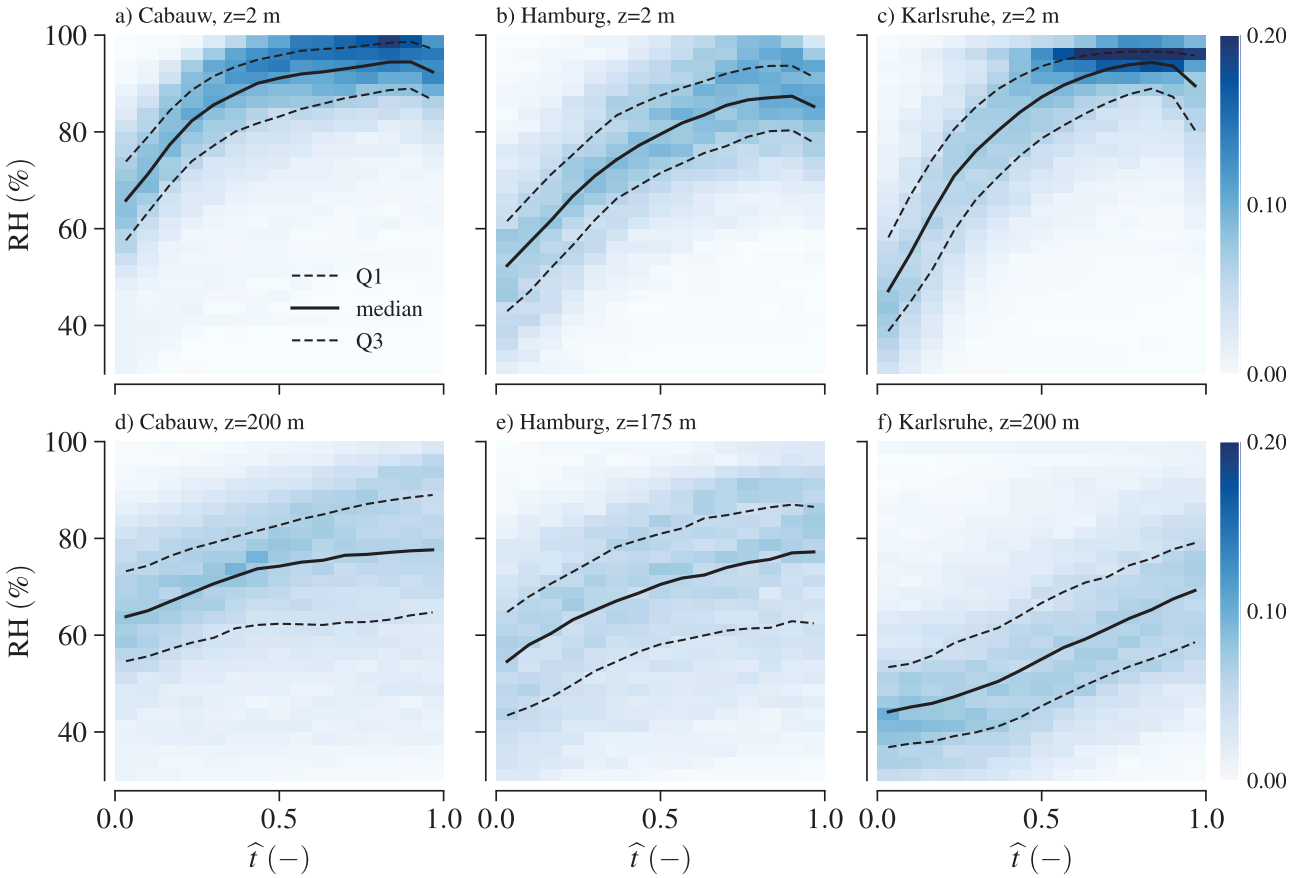

Figure 3. 2-D histograms of the relative humidity at (top) 2 m height and (bottom) ∼200 m height. The solid line indicates the median value, the dashes lines the interquartile range.

2.3.2. Temporal Evolution NBL

During the night, all sites show the strongest increase in RH near the surface, where Hamburg is most dry (Figure 3). Despite the large initial difference between Cabauw and Karlsruhe, the latter shows a stronger increase in RH during the night, resulting in similar early morning (median) relative humidities of 94–95%. As shown in Figure 4, the specific humidity tendencies during the night are small: for all three sites, the net and maximum differences between t_{N0} and t_{N1} are less than 1 g kg^{-1}. Fitzjarrald and Lala (1989) report similar findings as the results of limited mixing caused by valley dynamics, here it seems that neither evaporation or dew deposition is strong enough to make the specific humidity deviate from the initial well-mixed conditions. To quantify the contribution of these changes on the relative humidity, the relative humidity budget is studied (e.g., Ek & Mahrt, 1994):

$$\frac{\partial \mathrm{RH}}{\partial t} = \frac{\partial}{\partial t}\left(\frac{q}{q_s}\right) = \underbrace{\frac{1}{q_s}\frac{\partial q}{\partial t}}_{\delta q} - \underbrace{\frac{\mathrm{RH}}{q_s}\frac{\partial q_s}{\partial T}\frac{\partial T}{\partial t}}_{\delta T}, \tag{1}$$

where q_s is the saturation-specific humidity. The budget terms—indicating the change in relative humidity due to drying or moistening of the ABL (δq) and warming or cooling of the ABL (δT)—are calculated approximating the time derivatives as finite differences forward in time (with a 10 min data interval). A time integration of equation (1) then provides the relative contribution of the two different terms. To prevent an accumulation or growth of the error, we use the observed RH on the right hand side, instead of the numerically integrated RH. The results are shown in Figure 5. For all sites the drying of the near-surface layers contributes only ∼0–4% to the RH tendency, which is an order of magnitude less than the impact of NBL cooling.

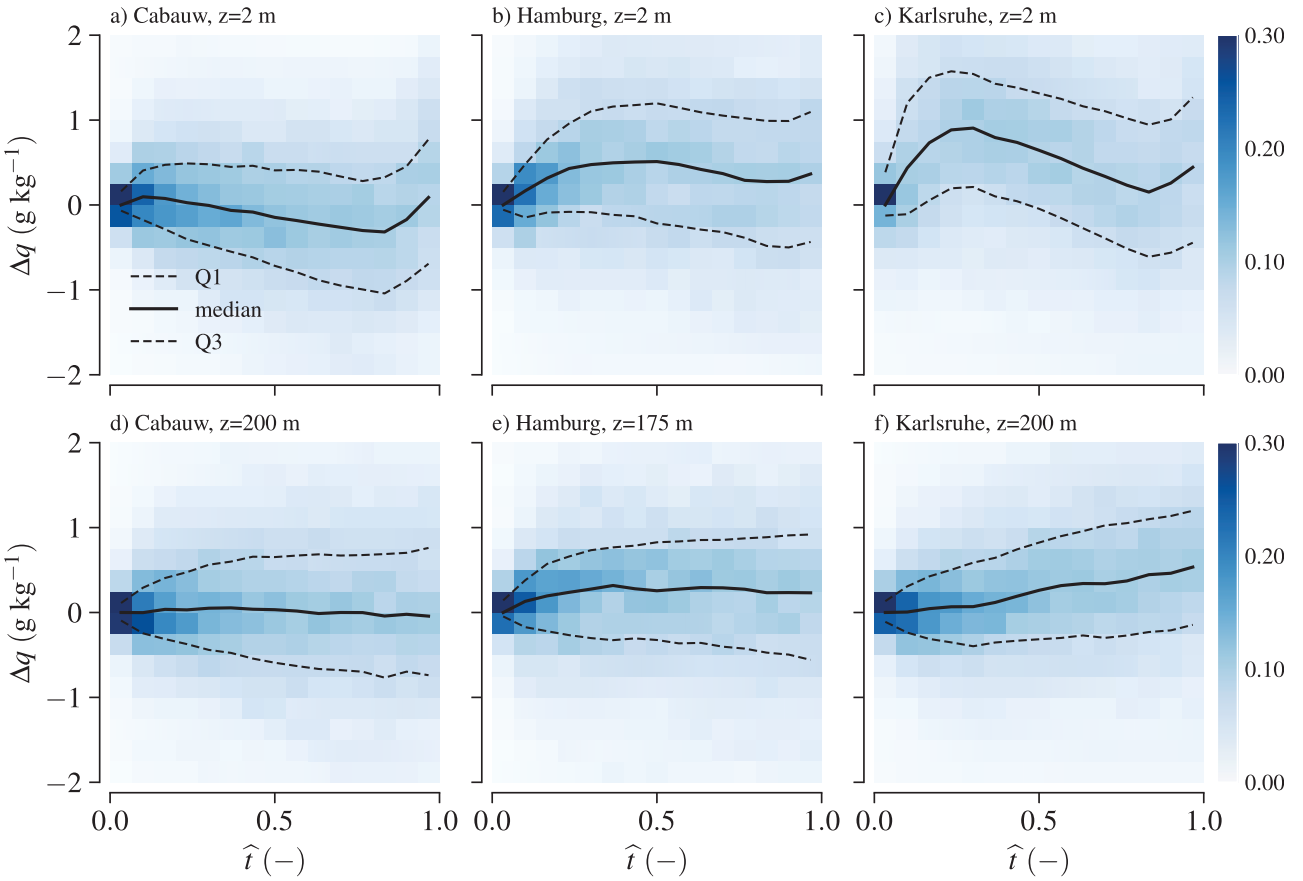

Figure 4. Like Figure 3, for the specific humidity.

2.4. Extremes During the Nocturnal Period

Although the two-dimensional histograms are useful to summarize the typical evolution of the NBL, it is difficult to obtain extremes from such figures. For example, for the relative humidity in Figure 3, the interesting details—how often does the NBL saturate?—are difficult to read. Furthermore, since extremes like the

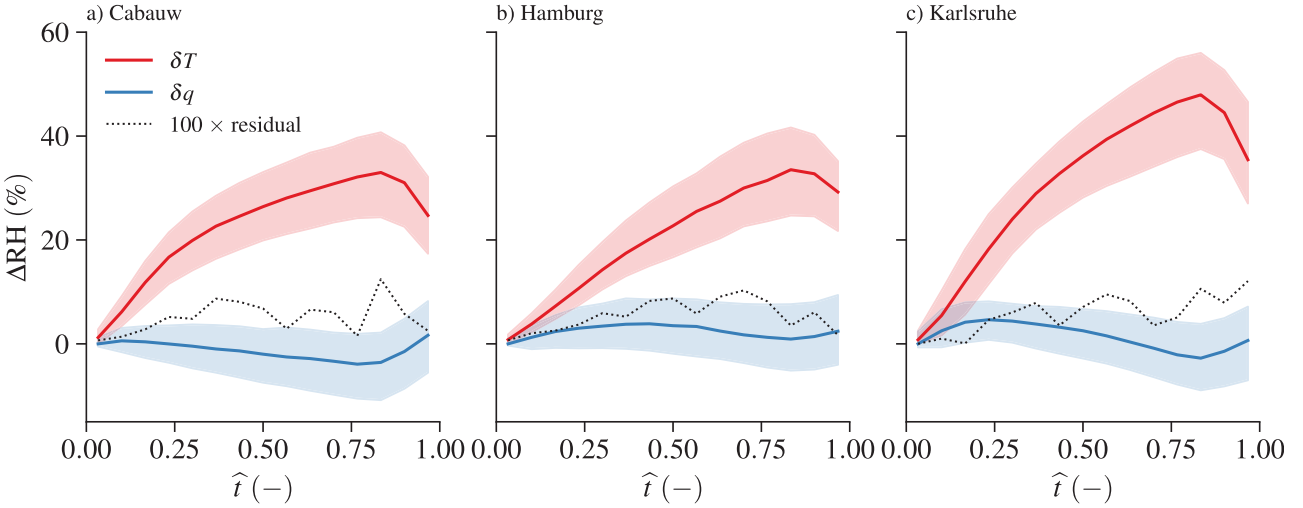

Figure 5. Relative humidity budget at 2 m height, derived using equation (1). δT is the contribution of changes in temperature, δq the changes due to changes in specific humidity, and the grey lines indicate the residual (diagnostic tendency minus prognostic tendency). Solid lines denote median values, the shaded area the interquartile range.

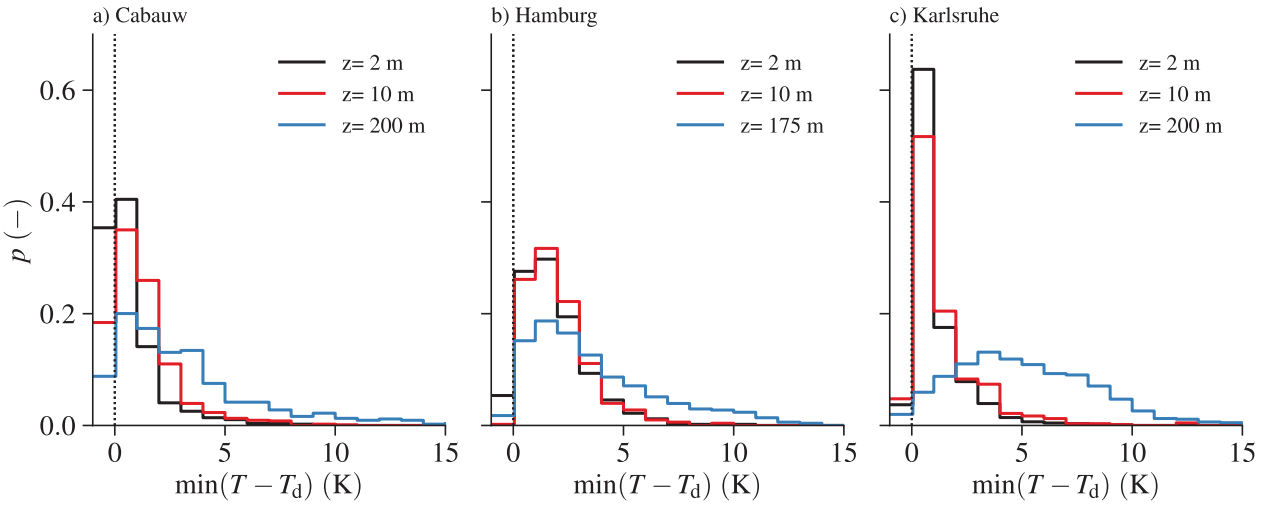

Figure 6. Histogram of minimum dew point depression between t_{N0} and t_{N1}. The first bin encloses all values from $-\infty < (T-T_d) \leq 0$ K.

maximum relative humidity do not necessarily occur at the same time during different nights, some details are lost.

As a more strict assessment of these extremes, Figure 6 shows histograms of the minimum dew point depression observed during all of the sampled nights. At 2 m height Cabauw frequently experiences conditions which are saturated, with a probability of 0.35, corresponding to a frequency of approximately once every three nights. These findings are in line with the direct visibility measurements (2011–2014, not shown). For Hamburg and Karlsruhe, the probability is lower: 0.05 (1/20 days) and 0.035 (1/28.6 days), respectively. For Cabauw the probability decreases with height, to 0.18 (1/5.6 days) at 10 m height and 0.08 (1/12.5 days) at 200 m height. For Karlsruhe the probability slightly increases at 10 m height to 0.045 (1/22.2 days). Considering that we have approximately 4×30 nights during the May through August period and analyze about 50% of them (Table 1), the frequency of finding a saturated night above 2 m height in Hamburg, or above 10 m height in Karlsruhe, is very small at about one night during this period.

Although saturated conditions at 200 m height (Hamburg: 175 m) in between convective days are only rarely observed, all sites are frequently close to saturation. For example, for the range $0 < T-T_d \leq 2$ K, the probabilities are 0.37 (1/2.7 days) for Cabauw, 0.34 (1/2.9 days) for Hamburg, and 0.14 (1/7.1 days) for Karlsruhe.

Summarized, even for the summer period—which is typically drier than the winter season–Northwest European nights are relatively moist. At 2 m height the late night median relative humidities are as high as 94–95% for Cabauw and Karlsruhe, and the strong increase in RH during the night is mostly governed by a decrease in temperature, where changes in specific humidity only play a minor role. Note that this might be a reflection of our selection criteria, where during clear nights the temperature tendency is expected to be larger than during cloudy nights, and hence a shift from δT to δq might be expected for cloudy nights. Despite the high relative humidities, only Cabauw (situated in a low and moist polder) frequently experiences saturation near the surface. Although the probability of finding saturated conditions decreases with height, the atmosphere at 200 m height is often within 2 K from saturation; conditions in which the negative temperature bias introduced by excessive vertical mixing (Figure 1) could results in the spurious formation of low clouds.

3. Implications of Mixing Biases on Nocturnal Low Clouds

The previous section showed that saturation at night most likely occurs near the surface. Given the positive near-surface temperature biases that arise from an overestimation of vertical mixing (Figure 1), these shallow layers of mist are likely absent in models. Furthermore, even in the absence of temperature (or other model) biases, the vertical grid spacing near the surface is likely insufficient to resolve mist with such a small (<10 m) vertical extent.

We postulate that the absence of such shallow mist layers in LES is unlikely to influence the NBL development, or convection during the following day. To explore this hypothesis, we studied the influence of fog/mist on the nocturnal radiation balance using an offline one-dimensional radiative transfer model (Pincus & Stevens, 2013, results not shown). By varying both the vertical extent (0–50 m) and liquid water content (0–0.5 g m^{-3}) of the fog layer, and comparing the net surface radiation with a clear sky experiment, it became clear that the observed shallow fog/mist layers influence the long-wave incoming radiation by only a few W m^{-2}. In addition, after sunrise these thin mist layers are insufficiently opaque to block the incoming shortwave radiation, and early morning surface heating typically causes a quick evaporation of such fog layers (e.g., Stull, 1988), so that their net effect on the overall energy budget is relatively small.

More interesting are the conditions where model biases have the potential to form spurious low clouds, as the NBL temperatures near or above the NBL top are underestimated (Figure 1) as the result over overestimating mixing. At least in theory, this could create deeper cloud layers which have a stronger impact on the nocturnal radiation budget, which can persist after sunrise, decreasing the incoming shortwave radiation, and delaying the development of the convective boundary layer (Anber et al., 2015; Yin et al., 2015).

To address whether model biases as illustrated in Figure 1 could cause spurious low clouds, we study the impact that overestimating vertical mixing has on the relative humidity in the NBL, using a conceptual model that approximates the typical NBL structure in LES. The conceptual model allows us to perform sensitivity experiments for a wide range of conditions, using only a fraction of the computational resources that would be required for running the same experiments in LES.

3.1. Description of the Conceptual Model

We consider a nocturnal boundary layer which develops from an idealized convective boundary layer (CBL, Figure 7a): a mixed layer of depth z_c, with a constant potential temperature $\langle\theta\rangle$ and specific humidity $\langle q\rangle$ (e.g., Lilly, 1968). For European conditions, z_c is typically around 1–2 km, with a mixed-layer top relative humidity (RH_c) often close to—but on average less than—100%. The initial relative humidity in the NBL is mostly governed by z_c and RH_c, with the highest relative humidities (most favorable for saturation during the night) arising from a shallow and relatively moist CBL. From z_c, $\langle\theta\rangle$, and RH_c, the bulk-specific humidity $\langle q\rangle$ can be calculated, which—based on the findings of section 2.3 and Fitzjarrald and Lala (1989)—is assumed to be constant in time throughout the night.

Unlike for convective conditions, where turbulence is typically strong enough to maintain well-mixed vertical profiles, the same assumption cannot be made for the change of potential temperature in the NBL. Depending on the amount of turbulence at night, two types of NBLs tend to form: If turbulence is weak and the development of the NBL is mostly driven by radiative cooling, concave upward potential temperature profiles (with

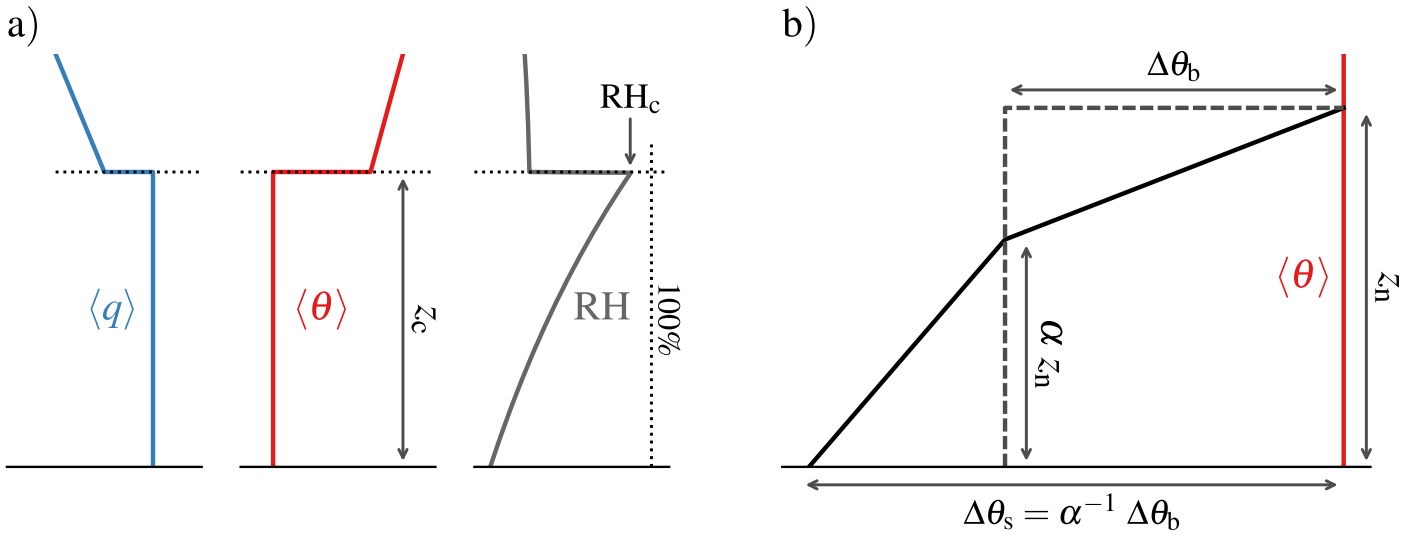

Figure 7. Sketch of (a) the initial convective conditions (e.g., Lilly, 1968) and (b) parameterization of the vertical potential temperature structure, given the bulk NLB cooling ($\Delta\theta_b$), the NBL depth (z_n), and a constant parameter α.

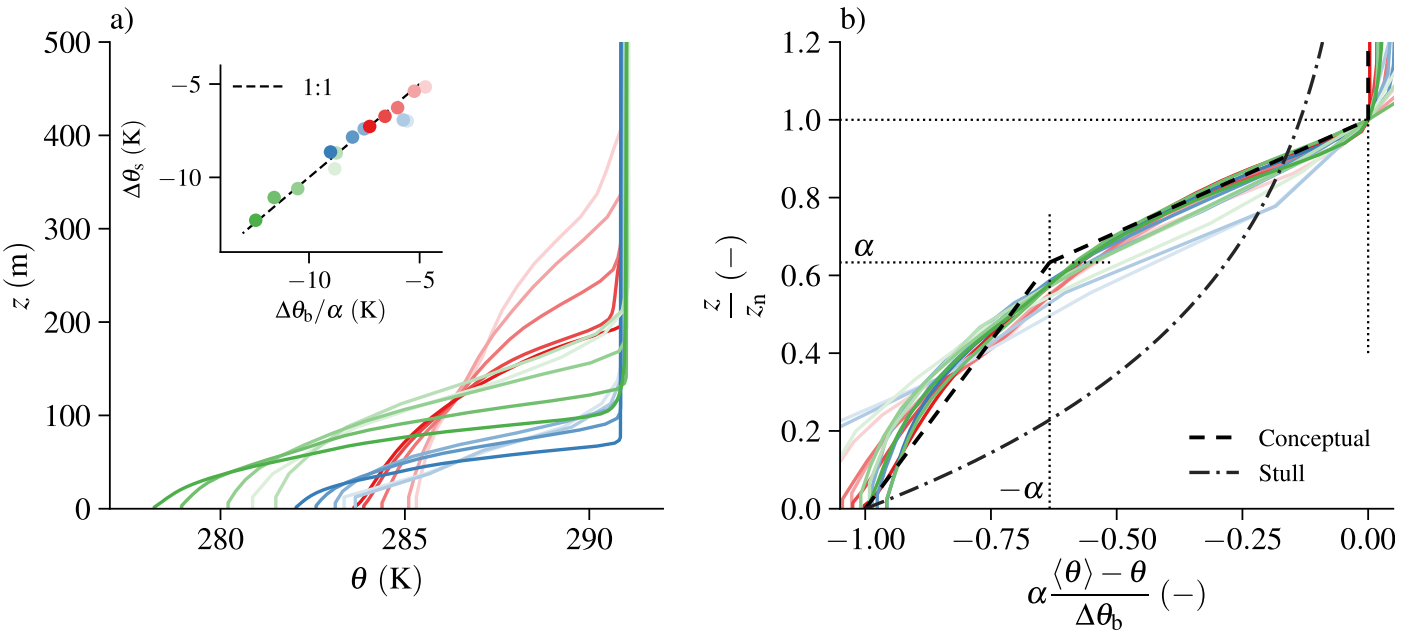

Figure 8. LES experiments from *vSS15*, (left) unscaled and (right) scaled (right). The three different colors indicate different (physical) experiments, the darkest lines high resolution LES experiments with a grid spacing of 3.125^3 m, the lightest colors low resolution LES experiments with a grid spacing of 100 × 100 × 25 m. The dashed line in (b) indicates the temperature structure that we assume, the dash-dotted line the temperature structure from Stull (2000).

the strongest temperature gradient near the surface) are formed (e.g., Stull, 1983a, 19832b, 2000). For more turbulent conditions, turbulent mixing creates slightly better well-mixed vertical profiles, with the strongest temperature gradients near the NBL top (e.g., Vogelezang & Holtslag, 1996). We adopt a vertical structure typical for turbulent conditions, as according to the classification proposed by Vogelezang and Holtslag (1996), 76.5–80% of the nights used in section 2 are of the turbulent kind, where $\partial^2\theta/\partial z^2 < 0$ over the depth of the NBL. This is confirmed by the maximum nighttime bulk Richardson numbers, with median near surface values of ∼0.05–0.07, and an interquartile range of ∼0.01–0.4, for Cabauw and Hamburg.

To determine the shape of the temperature profiles, we use the LES results from vSS15. These experiments were set up to cover the typical European conditions, and in addition, range from well to under-resolved LES experiments, with a grid spacing ranging from (Δx, Δy, Δz) 3.125 m × 3.125 m × 3.125 m to 100 m × 100 m × 25 m. Figure 8a shows the potential temperature profiles, analyzed at sunrise. The characteristics of the high-resolution experiments (darkest colors) range from boundary layer depths of 75 to 200 m, with potential temperature differences between the surface and residual layer of −7 K to −13 K. With increasing grid spacing (increasingly lighter colors), vertical mixing is progressively stronger overestimated, resulting in relative biases in the NBL depth as large as 100%. In section 3.2, such biases will be used as a controlling parameter to study how overestimating vertical mixing influences the RH in the NBL.

If we define the total NBL cooling in LES between t_{N0} and some arbitrary time t_1 later as:

$$\Delta Q = \int_{t_{N0}}^{t_1} (\overline{w'\theta'_s})\, \mathrm{d}t = \int_0^{z_n} [\theta(t_1, z) - \theta(t_{N0}, z)]\, \mathrm{d}z, \tag{2}$$

with z_n the depth of the stable boundary layer, the bulk cooling equals (Figure 7b):

$$\Delta\theta_b = \frac{\Delta Q}{z_n}. \tag{3}$$

As shown in the inset in Figure 8a, the potential temperature difference between the surface and residual layer ($\Delta\theta_s$, Figure 7) scales well with $\Delta\theta_b$, with the inclusion of some prefactor $\alpha = 1.9/3$. We try to approximate the NBL with a bilinear structure defined by $\Delta\theta_s$ and z_n. If we use these quantities to scale the potential temperature profiles, we find a universal shape for the vertical structure of the NBL, as shown in Figure 8b. Although the scaling sets the temperature at the surface ($\theta = \langle\theta\rangle + \alpha^{-1}\,\Delta\theta_b$) and NBL top ($\theta = \langle\theta\rangle$), it still

requires assumptions about the distribution of the total cooling with height (equation (2)). We propose a simple two layer structure, with the temperature at a height αz_n equal to $\langle\theta\rangle - \Delta\theta_b$ (Figure 7b). As shown in Figure 8b (dashed line), this gives a reasonable agreement with the LES experiments, without introducing too much complexity in the assumptions of the vertical NBL structure. We should stress that in the results from Figure 8, and the remainder of this study, α is fixed at $\alpha = 1.9/3$. Also included in Figure 8b is the parameterization proposed by Stull (2000):

$$\theta = \langle\theta\rangle - \Delta\theta_s \ e^{-z/H_e}, \tag{4}$$

where we used an e-folding height $H_e = 0.5 z_n$ for a best fit to the LES data. It is clear that the exponential shape is not appropriate for characterizing the biases that arise from insufficient resolution in the LES experiments of vSS15.

Summarized, given the total NBL cooling ΔQ and the NBL depth z_n (equation (3)), the conceptual model can reproduce the vertical potential temperature structure of the NBL. Given the results from Figure 8b, the model not only reproduces the vertical structure observed in high-resolution (well-resolved) LES, but also the change in structure as the NBL depth is overestimated as the result of overestimating vertical mixing. Assuming that the specific humidity is constant in both height and time (section 2.3), this additionally opens the possibility to study—for example—how quantities like the relative humidity are influenced by mixing biases.

3.2. Numerical Solutions

With the conceptual model, we can study how the vertical structure of the NBL changes in LES as a function of the nocturnal boundary layer depth z_n, where increasing z_n mimics the impact of overestimating vertical mixing as observed in low-resolution LES or many boundary layer parameterizations (e.g., Cuxart et al., 2006). We perform a number of experiments, starting from a convective boundary layer with conditions typical for northwestern Europe (Table 1). The initial conditions are listed in Table 2.

For the experiments, we vary two variables that influence the NBL structure: the total NBL cooling (ΔQ) and the NBL depth (z_n). ΔQ—in reality the result of both the radiative and turbulent flux divergence over the NBL—is here combined set by prescribing a fixed surface sensible heat flux H ($H = \overline{w'\theta'_s}\rho c_p$) over a time period $t_1 - t_{N0} = 32{,}400$ s (equation (2)). For each value of H, the NBL depth is varied to mimic mixing biases, the temperature profiles are reconstructed, and using $\langle q\rangle$ (constant in time) the relative humidity at the surface (RH_s) and at αz_n (RH_t) is calculated.

Figure 9a shows the resulting RH at the surface (solid lines) and at αz_n (dashed lines) as a function of z_n, for $H = \{-20, -40, -60\}$ W m^{-2}. The results are divided in two regimes: the top-left part where for a given z_n the RH is highest at the surface, and the bottom-right area where the RH is highest near the NBL top. A number of conclusions can be drawn from these experiments:

1. For conditions which are close to saturation, the surface RH is higher than the RH at αz_n, thus favoring saturation near the surface over low clouds, which is in line with the findings from section 2.
2. For almost all conditions, increasing z_n—which mimics the result of overestimating vertical mixing—results in a decrease in RH at both the surface and αz_n. This makes it unlikely that overestimating vertical mixing could cause a spurious formation of low clouds.
3. The only conditions where the RH at αz_n increases with a deepening NBL occur for weakly cooled and deep NBLs ($H = -20$ W m^{-2}, $z_n > 250$ m), for which the conditions are not close to saturation.

These results are easier to understand if we consider how the relative humidity changes as a function of z_n. At the surface, increasing z_n always results in a decrease in RH, so we will focus on the RH at αz_n (RH_t). The tendency at this height can be expressed as:

$$\frac{\partial RH_t}{\partial z_n} \approx \underbrace{\frac{RH}{q_s}\frac{\epsilon}{p}\frac{\partial e_s}{\partial T}\frac{\Delta Q}{z_n^2}}_{\delta\theta} + \underbrace{\frac{RH}{q_s}\frac{\epsilon}{p}\frac{\partial e_s}{\partial T}\frac{\alpha g}{c_p}}_{\delta T} - \underbrace{\frac{RH}{p}\alpha\rho g}_{\delta p}. \tag{5}$$

Here the symbols have their standard meanings (see Appendix B for a derivation). The tendency equation consists of three terms: the first term ($\delta\theta$) describes how the change in potential temperature—which by definition is positive as the NBL is deepened—decreases the

Table 2
Initial Conditions of the Numerical Experiments With the Conceptual Model

Description	Symbol	Value
Convective boundary layer depth	z_c	1,000 m
Bulk potential temperature CBL	$\langle\theta\rangle$	293 K
Bulk-specific humidity CBL	$\langle q\rangle$	8.3 g kg^{-1}
Relative humidity at z_c	RH_c	95%
Surface pressure	p_s	10^5 pa

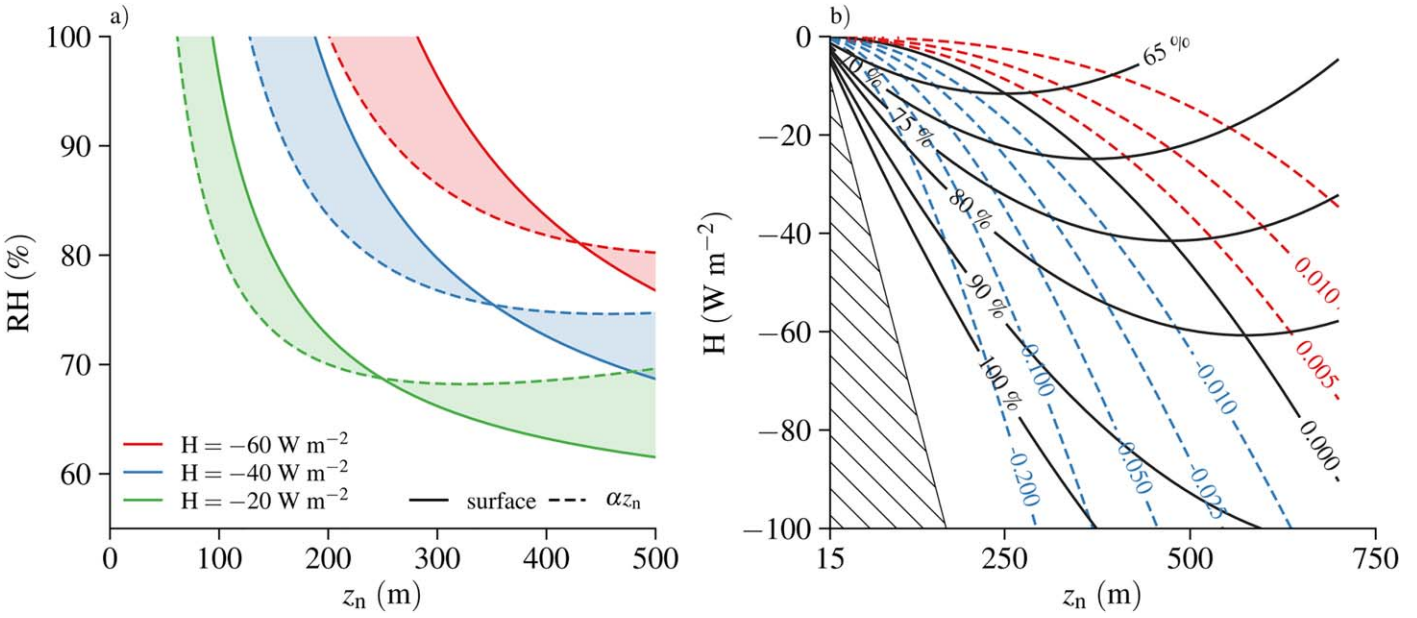

Figure 9. Experiments with the conceptual model, using the initial conditions from Table 2. (left) Relative humidity at the surface and αz_n for three different cases. (right) Relative humidity at αz_n (solid lines), and the total RH tendency calculated using equation (5) (dashed lines, in % s^{-1}).

relative humidity. As the relative humidity depends on the absolute temperature, the second term (δT) describes the influence of adiabatic cooling on the relative humidity, which by definition is a negative contribution to the RH budget. The last term (δp), which is small compared to the other two terms, describes the change in RH caused by the dependence of the saturation specific humidity on pressure.

In Figure 9b the relative humidity at $z=\alpha z_n$ (solid black contours), and its tendency as a function of z_n (colored dashed lines), are shown for a wide range of conditions. The initial conditions of the experiments are identical to the cases shown in Figure 9a (Table 2), and the results are again analyzed after a time period $t_1 - t_{N0} = 32{,}400$ s (9 h). Not all combinations of H and z_n are physically likely. For example, for the hatched area in Figure 9b, the surface cooling ($\Delta\theta_s$) over the night would be more than 25 K.

One prerequisite for a case where spurious deepening of the NBL results in saturation, is that the relative humidity at αz_n increases with increasing z_n. It is again clear that those conditions (dashed red lines) only occur for weakly cooled and/or deep NBLs, where the boundary layer top is far from saturation. For all conditions which are close to saturation, deepening the NBL would result in a decrease of RH_t.

We can study this behavior further if we consider the individual terms of equation (5), which are shown in Figure 10 for a case with a surface cooling H = −40 W m^{-2}. For a shallow NBL, the absolute temperature term (δT) is much weaker than the potential temperature term ($\delta\theta$), but as the latter decreases inverse proportional to the NBL depth squared, its contribution decreases quickly as the NBL is deepened. Only for $z_n > 450$ m the negative contribution from $\delta\theta$—caused by the increase in potential temperature at αz_n—become small enough so that it can be offset by the positive contribution from δT—caused by adiabatic cooling—so that further deepening of the NBL results in an increase in RH.

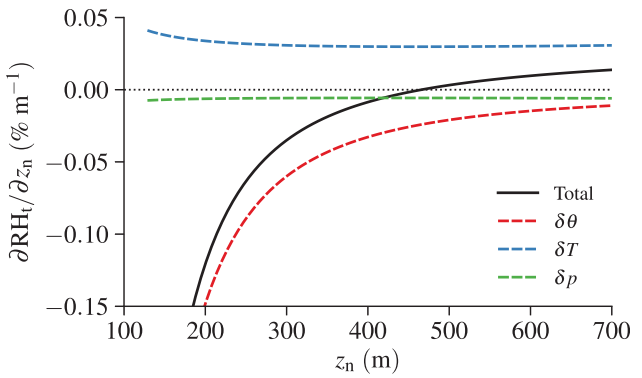

Figure 10. Budget terms of equation (5), for a case with H = −40 W m^{-2}.

We should add that in the numerical experiments, we assumed that the surface heat flux (H) is not influenced by biases in vertical mixing, while vSS15 found that overestimating vertical mixing typically lowers H. A sensitivity study with the conceptual model (not shown)–adding a reduction in the surface heat flux as a function of overestimating the NBL depth—showed that including a more realistic land-atmosphere coupling would not have influenced the main conclusions drawn from this section.

Summarized, the goal of the numerical experiments was to determine whether overestimating the NBL depth—as is typically the case when vertical mixing is overestimated—could results in saturation of the NBL. The numerical experiments indicate that this is unlikely: for conditions which are close to saturation, the highest relative humidities are found near the surface. In addition, for nearly all cases, deepening the NBL results in a decrease in relative humidity throughout the NBL.

4. Summary and Conclusions

We studied whether overestimating vertical mixing in the NBL is likely to produce low clouds or fog in LES, which do not occur in reality. Such an overestimation of vertical mixing, and consequently an overestimation of the NBL depth, is typical for low-resolution LES (low-resolution with respect to the grid spacing required to resolve nocturnal turbulence), but also for many boundary layer parameterizations based on the RANS equations. The resulting biases in the mean thermodynamic structure of the NBL typically consist of an overestimation of the near surface temperature, and underestimation of the temperatures near or above the NBL top, potentially causing an absence of fog/mist occurring in reality, or a spurious formation of low clouds near/above the NBL top. Such biases in low clouds have the potential to influence the energy budget in ways that did not occur in our earlier study of dry boundary layers (vSS15).

The question whether overestimating vertical mixing is likely to influence the formation of fog or low clouds was addressed using both observations and a new conceptual model developed to encapsulate the results from LES.

From the tower observations from Cabauw, Hamburg and Karlsruhe we only considered the summertime period (MJJA), and given the interest in how NBL biases might influence daytime convection, further subsampled the nights in between convective days. Even after subsampling the (convective) summertime conditions, the NBL is still surprisingly moist, with median early morning (sunrise) relative humidities at 2 m height as high as 94–95% for Cabauw and Karlsruhe. Most likely due to its close vicinity to the city, the early morning relative humidities in Hamburg are $\sim$ 10% lower. Higher up (200 m), the relative humidities are lower, typically around 70–80%. By studying the extremes during the nocturnal period, it became evident that only Cabauw frequently experiences saturated conditions near the surface, occurring roughly once every three nights. Given the positive near-surface temperature biases that arise from overestimating vertical mixing, and the small vertical extent of these fog/mist layers ($<$10 m), these events are likely unresolved in low-resolution LES. However, given their small vertical extent, we argued that this is unlikely to influence the energy budget and NBL development, or have an impact on the following day of convection.

The study of the nocturnal extremes also indicated that at 200 m height, the NBL is frequently within 2 K of saturation. With the negative temperature biases that arise from overestimating vertical mixing, this could potentially cause a spurious formation of low clouds, which—through their influence on the NBL energy budget—could have a larger impact on the development of the NBL, and the following day of convection. We addressed this question using a newly developed conceptual model which, given the total nocturnal cooling and NBL depth, realistically reproduces the vertical structure of the NBL as typically produced by LES. By varying the boundary layer depth—to mimic typical parameterization errors—for a given amount of cooling, this allowed us to study if overestimating vertical mixing could result in low clouds, for a wide range of conditions. The results indicate that a spurious formation of low clouds is unlikely to happen. First, for conditions which are close to saturation, the maximum RH is observed near the surface. Second, conditions where deepening the NBL results in an increase in the NBL top relative humidity only occur for weakly cooled and/or deep boundary layers, where the NBL top is far from saturation.

These results complement the findings from vSS15. For LES experiments of the diel cycle of convection, where the main focus is on daytime convection and where details of the nocturnal boundary layer are less important, the use of a resolution which is insufficient to resolve nocturnal turbulence is unlikely to influence daytime convection. This greatly relaxes the requirements on resolution, opening the possibility for LES of the diel cycle of convection on domains as large as hundreds or a thousand kilometer.

Appendix A: Sampling Criteria Measurement Data

We sample the nights in between relatively clear convective days by considering the observed short-wave incoming radiation over a period of 5–3 h before sunset, and 3–9 h after sunrise, and only select nights where

the mean incoming shortwave radiation over both periods is more than 40% of its theoretically maximum value (Stull, 1988, pp. 255–258). The period after sunrise was deliberately chosen longer, as with a shorter averaging period a number of convective days which started with clouds were filtered out. In addition, based on a visual inspection of the sampling, nights with a mean surface pressure tendency of less than (i.e., more negative) -20 pa h^{-1} are excluded, as those nights were typically dominated by frontal passages.

Appendix B: Derivation Relative Humidity Budget Equation

Assuming an air density which is constant with height and equal to the density at the surface, $\theta \approx T+(g/c_p)z$ (with g the gravitational acceleration and c_p the isobaric specific heat of air), and a surface pressure which is constant in time and equal to the reference pressure (10^5 Pa), the change in absolute temperature at the surface (subscript s) and αz_n (subscript t) changes with the NBL depth z_n as see (equation (3) and Figure 7b):

$$\frac{\partial T_s}{\partial z_n} = -\frac{\Delta Q}{\alpha z_n^2}, \tag{B1}$$

$$\frac{\partial T_t}{\partial z_n} \approx -\frac{\Delta Q}{z_n^2} - \frac{\alpha g}{c_p}. \tag{B2}$$

In general, the change in relative humidity (RH) with height equals:

$$\frac{\partial \mathrm{RH}}{\partial z} = \frac{\partial}{\partial z}\left(\frac{q}{q_s}\right) = \frac{1}{q_s}\frac{\partial q}{\partial z} - \frac{\mathrm{RH}}{q_s}\frac{\partial q_s}{\partial z}, \tag{B3}$$

where under well-mixed conditions, the first term on the RHS—containing the vertical gradient of q—is zero. The change in the saturation specific humidity (q_s) with height can be approximated by:

$$q_s \approx \frac{\epsilon e_s}{p}, \tag{B4}$$

$$\frac{\partial q_s}{\partial z} \approx \frac{\epsilon}{p}\frac{\partial e_s}{\partial T}\frac{\partial T}{\partial z} - \frac{q_s}{p}\frac{\partial p}{\partial z} \tag{B5}$$

$$\frac{\partial \mathrm{RH}}{\partial z} \approx -\frac{\mathrm{RH}}{q_s}\frac{\epsilon}{p}\frac{\partial e_s}{\partial T}\frac{\partial T}{\partial z} + \frac{\mathrm{RH}}{p}\frac{\partial p}{\partial z}, \tag{B6}$$

where ϵ is the ratio between the gas constant for dry air (R_d) and the gas constant for water vapor (R_v), and e_s is the saturation vapor pressure. At the surface, the last term of equation (B6) is zero, and using equation (B1) the tendency can be expressed as:

$$\frac{\partial \mathrm{RH}_s}{\partial z_n} = \frac{\mathrm{RH}}{q_s}\frac{\epsilon}{p}\frac{\partial e_s}{\partial T}\frac{\Delta Q}{\alpha z_n^2}. \tag{B7}$$

At the height αz_n, two terms contribute to the change of temperature (equation (B2)), and assuming $\partial p/\partial z = -\rho g$, the tendency can be written as:

$$\frac{\partial \mathrm{RH}_t}{\partial z_n} \approx \frac{\mathrm{RH}}{q_s}\frac{\epsilon}{p}\frac{\partial e_s}{\partial T}\frac{\Delta Q}{z_n^2} + \frac{\mathrm{RH}}{q_s}\frac{\epsilon}{p}\frac{\partial e_s}{\partial T}\frac{\alpha g}{c_p} - \frac{\mathrm{RH}}{p}\alpha\rho g \tag{B8}$$

Acknowledgments
This research was funded by the Federal Ministry of Education and Research in Germany (BMBF) through the research program *High Definition Clouds and Precipitation for Climate Prediction*—HD(CP)2 (FKZ: 01LK1202E). The authors thank the University of Hamburg, the Cabauw Experimental Site for Atmospheric Research (CESAR), and the Institute for Meteorology and Climate Research of Karlsruhe Institute of Technology (KIT) for providing the observations, Bert Holtslag and Gert-Jan Steeneveld for feedback on an early draft of this manuscript, and David Fitzjarrald and an anonymous reviewer for their constructive comments on the final manuscript. The Cabauw observations were obtained from www.cesar-database.nl, the observations from Hamburg (http://www.wettermast.uni-hamburg.de) and Karlsruhe (www.imk.kit.edu/messmast) were provided by the universities upon request.

References

Acevedo, O. C., & Fitzjarrald, D. R. (2001). The early evening surface-layer transition: Temporal and spatial variability. *Journal of the Atmospheric Sciences*, *58*(17), 2650–2667. https://doi.org/10.1175/1520-0469(2001)058 <2650:TEESLT >2.0.CO;2

Anber, U., Gentine, P., Wang, S., & Sobel, A. H. (2015). Fog and rain in the amazon. *Proceedings of the National Academy of Sciences of the United States of America*, *112*(37), 11,473–11,477. https://doi.org/10.1073/pnas.1505077112

Barlow, J. F. (2014). Progress in observing and modelling the urban boundary layer. *Urban Climate*, *10*, 216–240. https://doi.org/10.1016/j.uclim.2014.03.011

Beare, R. J., Macvean, M. K., Holtslag, A. A. M., Cuxart, J., Esau, I., Golaz, J., et al. (2006). An intercomparison of large-eddy simulations of the stable boundary layer. *Boundary-Layer Meteorology*, *118*(2), 247–272. https://doi.org/10.1007/s10546-004-2820-6

Betts, A. (1973). Non-precipitating cumulus convection and its parameterization. *Quarterly Journal of the Royal Meteorological Society*, *99*(419), 178–196. https://doi.org/10.1002/qj.49709941915

Brümmer, B., Lange, I., & Konow, H. (2012). Atmospheric boundary layer measurements at the 280 m high Hamburg weather mast 1995–2011: Mean annual and diurnal cycles. *Meteorologische Zeitschrift*, *21*(4), 319–335. https://doi.org/10.1127/0941-2948/2012/0338

Cuxart, J., A. A., Holtslag, R. J., Beare, E., Bazile, A., Beljaars, A., Cheng, L., et al. (2006). Single-column model intercomparison for a stably stratified atmospheric boundary layer. *Boundary-Layer Meteorology*, *118*(2), 273–303. https://doi.org/10.1007/s10546-005-3780-1

de Roode, S. R., Jonker, H. J., van de Wiel, B. J., Vertregt, V., & Perrin, V. (2017). A diagnosis of excessive mixing in smagorinsky subfilter-scale turbulent kinetic energy models. *Journal of the Atmospheric Sciences*, *74*(5), 1495–1511. https://doi.org/10.1175/JAS-D-16-0212.1

Duynkerke, P. G. (1999). Turbulence, radiation and fog in Dutch stable boundary layers. *Boundary-Layer Meteorology*, *90*(3), 447–477. https://doi.org/10.1023/A:1026441904734

Edwards, J. (2009). Radiative processes in the stable boundary layer: Part I. Radiative aspects. *Boundary-Layer Meteorology*, *131*(2), 105–126. https://doi.org/10.1007/s10546-009-9364-8

Ek, M., & Mahrt, L. (1994). Daytime evolution of relative humidity at the boundary layer top. *Monthly Weather Review*, *122*, 2709–2721. https://doi.org/10.1175/1520-0493(1994)122 <2709:DEORHA >2.0.CO;2

Fitzjarrald, D. R., & Lala, G. G. (1989). Hudson valley fog environments. *Journal of Applied Meteorology and Climatology*, *28*(12), 1303–1328. https://doi.org/10.1175/1520-0450(1989)028 <1303:HVFE >2.0.CO;2

Garratt, J. R., & Brost, R. A. (1981). Radiative cooling effects within and above the nocturnal boundary layer. *Journal of the Atmospheric Sciences*, *38*(12), 2730–2746. https://doi.org/0.1175/1520-0469(1981)038 <2730:RCEWAA >2.0.CO;2

Heinze, R., Dipankar, A., Carbajal Henken, C. C., Moseley, C., Sourdeval, O., Trömel, S., et al. (2016). Large-eddy simulations over Germany using ICON: A comprehensive evaluation. *Quarterly Journal of the Royal Meteorological Society*, *143*, 69–100. https://doi.org/10.1002/qj.2947

Heinze, R., Moseley, C., Böske, L. N., Muppa, S. K., Maurer, V., Raasch, S., et al. (2017). Evaluation of large-eddy simulations forced with mesoscale model output for a multi-week period during a measurement campaign. *Atmospheric Chemistry and Physics*, *17*(11), 7083–7109. https://doi.org/10.5194/acp-17-7083-2017

Hohenegger, C., Schlemmer, L., & Silvers, L. (2015). Coupling of convection and circulation at various resolutions. *Tellus Series A*, *67*, https://doi.org/10.3402/tellusa.v67.26678

Holtslag, A. A. M., Svensson, G., Baas, P., Basu, S., Beare, B., Beljaars, A. C. M., et al. (2013). Stable atmospheric boundary layers and diurnal cycles: Challenges for weather and climate models. *Bulletin of the American Meteorological Society*, *94*(11), 1691–1706. https://doi.org/10.1175/BAMS-D-11-00187.1

Kalthoff, N., & Vogel, B. (1992). Counter-current and channelling effect under stable stratification in the area of Karlsruhe. *Theoretical and Applied Climatology*, *45*(2), 113–126. https://doi.org/10.1007/BF00866400

Kuttler, W., Weber, S., Schonnefeld, J., & Hesselschwerdt, A. (2007). Urban/rural atmospheric water vapour pressure differences and urban moisture excess in Krefeld, Germany. *International Journal of Climatology*, *27*(14), 2005–2015.

Lilly, D. K. (1968). Models of cloud-topped mixed layers under a strong inversion. *Quarterly Journal of the Royal Meteorological Society*, *94*(401), 292–309. https://doi.org/10.1002/qj.49709440106

Mauritsen, T., Svensson, G., Zilitinkevich, S. S., Esau, I., Enger, L., & Grisogono, B. (2007). A total turbulent energy closure model for neutrally and stably stratified atmospheric boundary layers. *Journal of the Atmospheric Sciences*, *64*(11), 4113–4126. https://doi.org/10.1175/2007JAS2294.1

Neggers, R. A. J., Siebesma, A. P., & Heus, T. (2012). Continuous single-column model evaluation at a permanent meteorological supersite. *Bulletin of the American Meteorological Society*, *93*(9), 1389–1400. https://doi.org/10.1175/BAMS-D-11-00162.1

Pincus, R., & Stevens, B. (2013). Paths to accuracy for radiation parameterizations in atmospheric models. *Journal of Advances in Modeling Earth Systems*, *5*, 225–233. https://doi.org/10.1002/jame.20027

Schalkwijk, J., Jonker, H. J., Siebesma, A. P., & Bosveld, F. C. (2015a). A year-long large-eddy simulation of the weather over Cabauw: An overview. *Monthly Weather Review*, *143*(3), 828–844. https://doi.org/10.1175/MWR-D-14-00293.1

Schalkwijk, J., Jonker, H. J., Siebesma, A. P., & Van Meijgaard, E. (2015b). Weather forecasting using GPU-based large-eddy simulations. *Bulletin of the American Meteorological Society*, *96*(5), 715–723. https://doi.org/10.1175/BAMS-D-14-00114.1

Stevens, B. (2006). Bulk boundary-layer concepts for simplified models of tropical dynamics. *Theoretical and Computational Fluid Dynamics*, *20*(5–6), 279–304. https://doi.org/10.1007/s00162-006-0032-z

Stull, R. B. (1983a). A heat-flux history length scale for the nocturnal boundary layer. *Tellus Series A*, *35*(3), 219–230. https://doi.org/10.3402/tellusa.v35i3.11435

Stull, R. B. (1983b). Integral scales for the nocturnal boundary layer. Part 1: Empirical depth relationships. *Journal of Climate and Applied Meteorology*, *22*(4), 673–686. https://doi.org/10.1175/1520-0450(1983)022 <0673:ISFTNB >2.0.CO;2

Stull, R. B. (1988). *An introduction to boundary layer meteorology*. Dordrecht, the Netherlands: Kluwer Academic Publishers.

Stull, R. B. (2000). *Meteorology for scientists and engineers*. Pacific Grove, CA: Brooks/Cole.

Tennekes, H. (1973). A model for the dynamics of the inversion above a convective boundary layer. *Journal of the Atmospheric Sciences*, *30*(4), 558–567. https://doi.org/10.1175/1520-0469(1973)030 <0558:AMFTDO >2.0.CO;2

Van de Wiel, B., Ronda, R., Moene, A., De Bruin, H., & Holtslag, A. (2002). Intermittent turbulence and oscillations in the stable boundary layer over land. Part i: A bulk model. *Journal of the Atmospheric Sciences*, *59*(5), 942–958. https://doi.org/10.1175/1520-0469(2002)059 <0942:ITAOIT >2.0.CO;2

van Stratum, B. J. H., & Stevens, B. (2015). The influence of misrepresenting the nocturnal boundary layer on idealized daytime convection in large-eddy simulation. *Journal of Advances in Modeling Earth Systems*, *7*, 423–436. https://doi.org/10.1002/2014MS000370

Van Ulden, A. P., & Wieringa, J. (1996). Atmospheric boundary layer research at Cabauw. *Boundary-Layer Meteorology*, *78*(1–2), 39–69. https://doi.org/10.1023/A:1026441904734

Vogelezang, D., & Holtslag, A. (1996). Evaluation and model impacts of alternative boundary-layer height formulations. *Boundary-Layer Meteorology*, *81*(3–4), 245–269. https://doi.org/10.1007/BF02430331

Yin, J., Albertson, J. D., Rigby, J. R., & Porporato, A. (2015). Land and atmospheric controls on initiation and intensity of moist convection: Cape dynamics and lcl crossings. *Monthly Weather Review*, *51*(10), 8476–8493. https://doi.org/10.1002/2015WR017286